frontiers in Materials

ORIGINAL RESEARCH
published: 18 June 2021
doi: 10.3389/fmats.2021.705930

B, N Dual Doped Coral-Like Carbon Framework With Superior Pseudocapacitance and Surface Wettability

Lu Han[1†], Xu Chen[2†], Shijie Zeng[2], Jia Liu[2], Zhongli Yang[1], Zhiqiang Wang[2], Liang Li[2], Haibao Wang[2], Zhanbin Hou[2] and Min Xu[1]*

[1]School of Physics and Electronic Science and Shanghai Key Laboratory of Magnetic Resonance, East China Normal University, Shanghai, China, [2]Beijing Smart-Chip Microelectronics Technology Co., Ltd., Beijing, China

Carbon-based materials are usually considered as conventional electrode materials for supercapacitors (SCs), therefore it is meaningful to enhance supercapacitive capacity and cycling stability *via* rational surface structure design of carbon-based materials. The bio-inspired coral-like porous carbon structure has attracted much attention recently in that it can offer large surface area for ion accommodation and favor ions-diffusion, promoting its energy storage capacity. Herein, we designed a superiorly hydrophilic B, N dual doped coral-like carbon framework (BN-CCF) and studied its surface wettability *via* low-field nuclear magnetic resonance relaxation technique. The unique coral-like micro-nano structure and B, N dual doping in carbon framework can enhance its pseudocapacitance and improve surface wettability. Therefore, when used as electrodes of SCs, the BN-CCF displays 457.5 F g^{-1} at 0.5 A g^{-1}, even when current density increases 20 folds, it still exhibits high capacitance retention of 66.1% and superior cycling stability. The symmetrical SCs assembled by BN-CCF electrodes show a high energy density of 14.92 Wh kg^{-1} (600 W kg^{-1}). In this work, simple structural regulation with B, N dual doping and surface wettability should be considered as effective strategy to enhance energy storage capacity of carbon-based SCs.

Keywords: coral-like carbon framework, B, N dual doping, pseudocapacitance, surface wettability, supercapacitors

OPEN ACCESS

Edited by:
Xingtao Xu,
National Institute for Materials Science, Japan

Reviewed by:
Junfeng Li,
Shanghai Maritime University, China
Yanjiang Li,
Suzhou University, China

***Correspondence:**
Min Xu
xumin@phy.ecnu.edu.cn

†These authors have contributed equally to this work

Specialty section:
This article was submitted to Carbon-Based Materials, a section of the journal Frontiers in Materials

Received: *06 May 2021*
Accepted: *04 June 2021*
Published: *18 June 2021*

Citation:
Han L, Chen X, Zeng S, Liu J, Yang Z, Wang Z, Li L, Wang H, Hou Z and Xu M (2021) B, N Dual Doped Coral-Like Carbon Framework With Superior Pseudocapacitance and Surface Wettability. Front. Mater. 8:705930. doi: 10.3389/fmats.2021.705930

INTRODUCTION

Supercapacitors (SCs), an emerging energy storage device, have been considered as supplement of rechargeable batteries, exhibiting superior energy storage, rapid charge/discharge rate and long cycling stability (Jian et al., 2019; Zhu et al., 2019; Hu et al., 2020; Reece et al., 2020). In different types of SCs, carbon materials have been most diffusely investigated and considered as active materials, especially in electrical double layer capacitors (EDLCs), characterized by low cost, excellent conductivity and stable chemical property (Gu et al., 2019; Huo et al., 2019; Lai et al., 2021; Li et al., 2021). However, due to the fast physical sorption rates of charges on the surfaces of active materials, carbon-based SCs display superior power density and long life span, but unsatisfying and limited energy density (5–10 Wh kg^{-1}) (Yi et al., 2014; Wang et al., 2018). In order to address this issue and extend applications of carbon-based SCs, improving their energy density *via* optimizing and designing carbon-based electrode materials was considered an effective way in recent years (Chang et al., 2018; Li et al., 2019a; Zhang et al., 2019; Cheng et al., 2020; Chen et al., 2021). Some

effective strategies have improved the capacitance of carbon electrode materials, involving the design of micro-nano structure with unique morphology or pore distribution (Liu et al., 2018b; Du et al., 2019). Among various nanostructures, the bio-inspired coral-like porous structure has attracted much attention since its peculiar dendritic architecture can provide large surface area for convenient exchange of substances and favor ions-diffusion in electrolyte, promoting its energy storage capacity (Wang et al., 2013). Osman et al. prepared coral structured porous-like carbon, displaying a superior specific capacitance of 360 F g^{-1} (1 mV s^{-1}) and 322 F g^{-1} (1 A g^{-1}) respectively (Osman et al., 2019). Yue et al. prepared coral-like carbons and when used as electrodes in SCs, they exhibited 360 F g^{-1} at 0.5 A g^{-1}, and excellent long cycling stability, due to their coral-like interconnected network structure (Yue et al., 2020).

Another attractive way is to introduce or enhance pseudocapacitance *via* doping heteroatoms into carbon frameworks. Sun et al. reported B-doped porous carbon nanoparticles, which displayed a gravimetric capacitance of 277 F g^{-1} at 1 A g^{-1} (Sun et al., 2018). Li et al. synthesized uniform N-doped porous carbon spheres with a gravimetric capacitance up to 247 F g^{-1} at 1 A g^{-1} (Li et al., 2019b). Li et al. prepared S-doped carbon aerogel with high specific capacitances of 335 and 217 F g^{-1} (1 A g^{-1}) in the aqueous and organic electrolytes (Li et al., 2019c). Due to the similar atomic radii of B and N with C atom, they can enter into carbon lattice easily, exhibiting superior advantage over other doping elements (such as P and S) (Zhao and Xie, 2018). Notably, electronic structure and density of carbon can be changed more significantly via B, N dual doping, compared with single heteroatom doping. (Ling et al., 2015; Zhang et al., 2015; Chen et al., 2017; Xia et al., 2017). Geng et al. synthesized B, N dual doped 2D porous carbon nanosheets exhibited gravimetric capacitance of 311 F g^{-1} at 0.2 A g^{-1} (Geng et al., 2019). Guo et al. prepared B, N dual doped porous carbon foam with an ultrahigh capacitance of 402 F g^{-1} at 0.5 A g^{-1} (Guo et al., 2018). These excellent supercapacitive performances mainly attributed to the structure regulation and pseudocapacitance contribution caused by B, N dual doping in carbon frameworks.

Besides the factor mentioned above, for carbon-based materials, hydrophilicity that can facilitate the ion diffusion and increase the ion-accessible surface area, which should also be taken into consideration (Zhao et al., 2015; Sun et al., 2018). Since pure carbon materials are normally hydrophobic, the surface wettability is a very critical factor for performance of carbon-based SCs (Zhao et al., 2015). Introducing hydrophilic functional groups (epoxy, carbonyl, and so on) and doping heteroatoms are two recognized strategies to improve the surface wettability of carbons. Yoo et al. reported carbon materials modified by sulfo group as high-performance electrodes of SCs to achieve a good electrolyte affinity (Yoo et al., 2014). Su et al. prepared hydrophilic porous carbide-derived carbons with N, Cl dual doping for high-performance SCs (Su et al., 2018). Wang et al. synthesized N, S dual doped porous carbon nanobowls, and found that N, S dual doping could increase carbon surface affinity toward electrolyte (Wang et al., 2018). Similarly, B, N dual doping should also improve the wettability of carbon-based electrode *via* significantly changing electronic density and structure of carbon (Saha et al., 2015; Wang et al., 2018; Zhao and Xie, 2018). Considering the above aspects, synergistically designing coral-like structure with regulated surface wettability and pseudocapacitance *via* B, N dual doping should be effective in improving the supercapacitive performance of carbon. However, relevant studies have seldom reported by now.

In this study, we prepared superiorly hydrophilic B, N dual doped coral-like carbon framework (BN-CCF) *via* a simple and efficient calcinating method, as shown in **Figure 1**. When used as electrodes of SCs, the BN-CCF displays outstanding excellent electrochemical performances. Besides, the symmetrical SCs assembled by BN-CCF electrodes shows satisfactory energy and power density. We even investigated the wettability of BN-CCF toward electrolyte by low-field nuclear magnetic resonance relaxation (LF-NMR) technique. Due to the unique coral-like micro-nano structure and the presence of B-containing groups (B-O, BC_2O, BCO_2, and B-N-C), the pseudocapacitance contribution and surface wettability can be improved in BN-CCF, which are mainly responsible for its superior supercapacitive performance.

EXPERIMENTAL SECTION

Material Synthesis

5 g of urea, 0.5 g of PEG-2000, and 0.05 g boric acid were dissolved in 50 ml of deionized water under stirring for 30 min. Subsequently, the mixture solution was dried to form a white precursor in an oven at 120°C for 10 h. Then, the precursor was annealed at 900°C with a heating rate of 5°C min^{-1} for 2 h under N_2 atmosphere in tube furnace. The prepared black powder was collected and washed with dilute hydrochloric acid to remove boron trioxide species. The obtained sample was named as BN-CCF. While, the N doped carbon framework (N-CF) was prepared using 5 g of urea and 0.5 g of PEG-2000 following the same synthesis process above for comparison.

The corresponding parameters of electrochemical measurement, material characterizations, dynamic water contact angle measurement and LF-NMR measurement have been detailedly described in the ESI.

RESULTSAND DISCUSSION

N-CF and BN-CCF were characterized by scanning electron microscopy (SEM) to analyze their surface structures and morphologies. N-CF exhibits an irregular and aggregate structure in **Figures 2A,B**, leading to insufficient contact between electrode and electrolyte, which is not beneficial to charge exchange at the interface. BN-CCF displays novel coral-like morphology in **Figures 2C,D**. Just like the coral in the sea, such a dendritic network structure can provide rich ion storage sites and lager ion-accessible surface area, which is

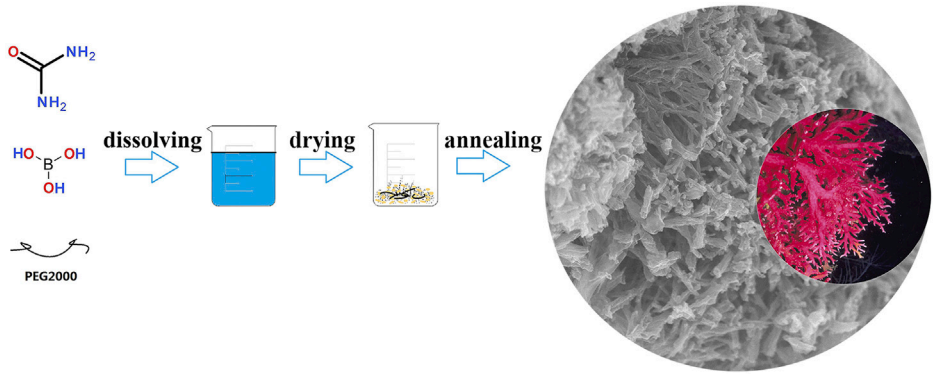

FIGURE 1 | Schematic of the synthesis process of BN-CCF.

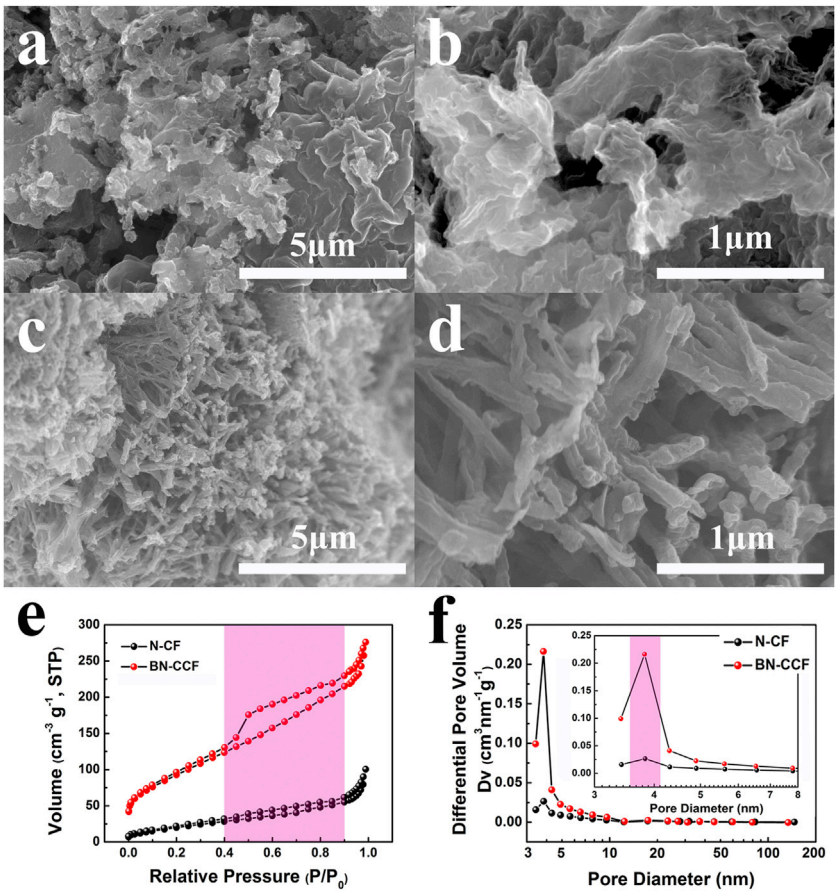

FIGURE 2 | SEM images of **(A,B)** N-CF and **(C,D)** BN-CCF **(E)** Nitrogen adsorption-desorption isotherms and **(F)** pore size distribution curves of N-CF and BN-CCF.

beneficial to the supercapacitive performance. As shown in **Figure 2E**, nitrogen adsorption-desorption isotherms of N-CF and BN-CCF show typical IV curves with a hysteresis loop ($0.40 < P/P_0 < 0.90$), indicating the existence of mesopores (2–50 nm) (Zhao et al., 2015). In **Figure 2F**, the pore size distribution curves has also confirmed the presence of mesopores. And in **Table 1**, it is found that BN-CCF displays a much higher surface area than N-CF, this benefits from its unique coral-like structure, benefitting the ion diffusion during the charge/discharge process, thus improving its supercapacitive performance.

TABLE 1 | Specific surface areas, mean pore diameters and pore volumes of N-CF and BN-CCF.

Sample	Specific surface area ($m^2\ g^{-1}$)	Mean pore diameter (nm)	Pore volume ($cm^3\ g^{-1}$)
N-CF	51.11	3.831	0.132
BN-CCF	224.7	3.818	0.336

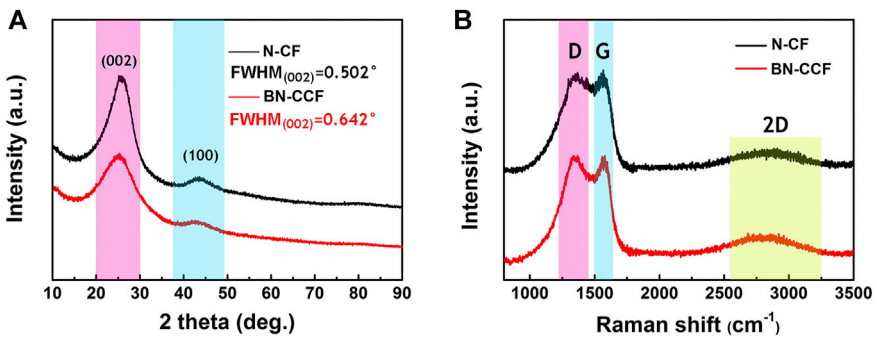

FIGURE 3 | (A) XRD patterns and **(B)** Raman spectra of N-CF and BN-CCF.

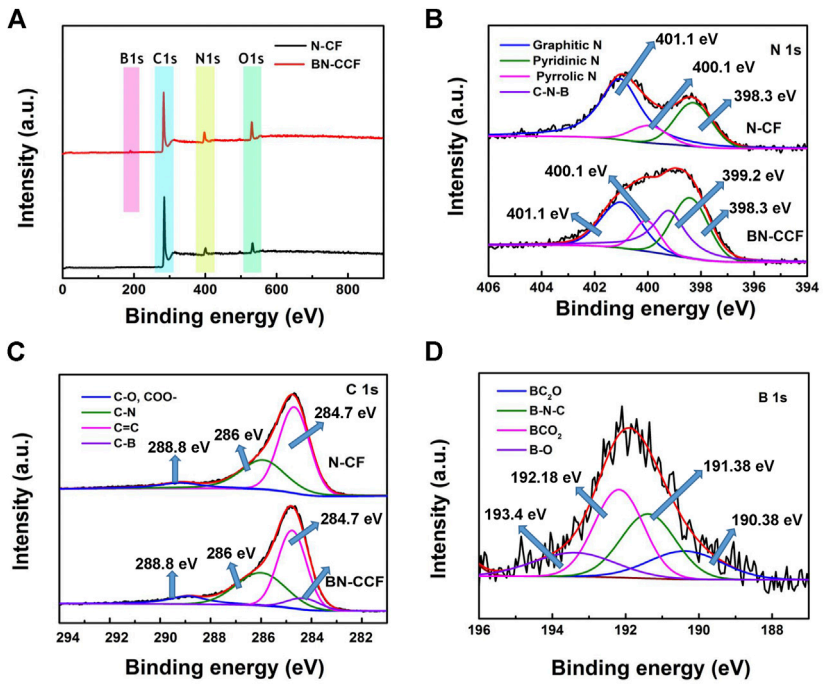

FIGURE 4 | (A) XPS survey spectra of N-CF and BN-CCF **(B)** N 1s and **(C)** C 1s XPS spectra of N-CF and BN-CCF **(D)** B 1s XPS spectrum of BN-CCF.

As shown in **Figure 3A**, X-ray diffraction patterns (XRD) of N-CF and BN-CCF, two broad characteristic humps (25° and 43°) can be observed, representing the (002) and (100) planes of carbon in N-CF and BN-CCF (JPCS no.41–1,487) (Hao et al., 2018), respectively. Besides, compared to N-CF, the peak width at half maxima of BN-CCF becomes larger, indicating more defects in BN-CCF. These defects are mainly caused by structural heteroatoms and stacks in sp^2-bonded conjugated graphitic carbons (Wang et al., 2018). In **Figure 3B**, D (1,350 cm^{-1}) and G (1,560 cm^{-1}) can be found in the Raman spectra of N-CF and BN-CCF, the corresponding intensity ratios of I_D/I_G can be used to evaluate their graphitization degree (Ling et al., 2016; Liu et al.,

TABLE 2 | Contents of B, N, C, and O in N-CF and BN-CCF.

Sample	B (at %)	N (at %)	C (at %)	O (at %)
N-CF	0	8.39	84.98	6.63
BN-CCF	6.2	11.32	72.28	10.2

2018a; Zhang et al., 2018). The I_D/I_G ratios of N-CF and BN-CCF are 0.97 and 1.01, respectively. BN-CCF show more disorders and defects in sp^2-bonded conjugated graphitic carbons. In other words, compared with N-CF, introducing boric acid in the precursor during the preparation can lead to lower graphitization degree in BN-CCF. This result is consistent with XRD analysis, the broader XRD peaks of (002) and (100) in BN-CCF indicate its enhanced amorphous state. These defects arising from B, N dual doping result in surface heterogeneity and superior hydrophilicity of carbon (Hao et al., 2015).

X-ray photoelectron spectroscopy (XPS) measurement was used to further investigate the heteroatoms in N-CF and BN-CCF, involving their species, contents and chemical bonds. As shown in **Figure 4A**, survey spectrum of BN-CCF clearly indicate the presence of B and N. The atomic ratios in N-CF and BN-CCF are listed in **Table 2**. The B contents in N-CF and BN-CCF are 0 and 6.2%, respectively. Interestingly, during B doping in BN-CCF, N and O contents increase. The detailed reason is still to be further investigated. Besides, there are three similar peaks at about 398.3, 400.1, and 401.1 eV in N 1s XPS spectra, revealing the co-existence of pyridinic N (N-6), pyrrolic N (N-5), and graphitic N (N-G). Notably, in N 1s XPS spectrum of BN-CCF, an additional peak at 399.2 eV indicate C-N-B bonds in carbon. In **Figure 4C**, three peaks at about 284.7, 286, and 288.8 eV can be observed in C 1s XPS spectra of BN-CF and BN-CCF, demonstrating the co-existence of C-C, C-N and C-O (COO-) bonds. In addition, C-B bond at around 284.3 eV can be found in BN-CCF, which is confirmed B doping in carbon (Hao et al., 2018; Wang et al., 2018). In particular, the peaks centered at about 288.8 eV (C-O, COO-) in BN-CCF become gradually prominent, meaning that B doping could increase carbon-oxygen group species. The fitted four peaks at 190.38, 191.38, 192.18, and 193.40 eV in B 1s XPS spectrum of BN-CCF (**Figure 4D**) are attribute to BC_2O, B-N-C, BCO_2, and B-O bonds, respectively. Based on the above analysis, B and N have successfully doped in carbon framework. Due to the inequable bond lengths of N-B and C-N in BN-CCF, structural distortion of graphitic carbon occurred and can be observed in XRD and Raman measurements (Wang et al., 2018). B doping in BN-CCF can be recognized as B-O, BC_2O, BCO_2, and B-N-C bonds (Hao et al., 2018). These B-containing groups can significantly change surface polarity, heterogeneity and electron distribution of carbons, enhancing the pseudocapacitance and wettability of BN-CCF framework (Wang et al., 2018; Zhao and Xie, 2018).

As illustrated in **Figure 5A**, in order to investigate the surface wettability of N-CF and BN-CCF, the dynamic water contact angle measurement was performed. The BN-CCF is hydrophilic with the initial contact angle of 82.48° and the droplet is completely spreaded within 30 s, while the droplet on N-CF remains almost unchanged for 30 s or longer. The introduction of B heteroatom in BN-CCF offers the B-containing groups (B-O, BC_2O, BCO_2, and B-N-C) that are expected to enhance the wettability of BN-CCF electrode toward electrolyte. To further study the surface hydrophilicity of N-CF and BN-CCF, LF-NMR technique was used for further analysis. This technique is useful in measuring parameters such as T_2 relaxation time which is sensitive to molecular motion (Li et al., 2017; Wiesman et al., 2018; Xiao et al., 2018). **Figure 5B** shows T_2

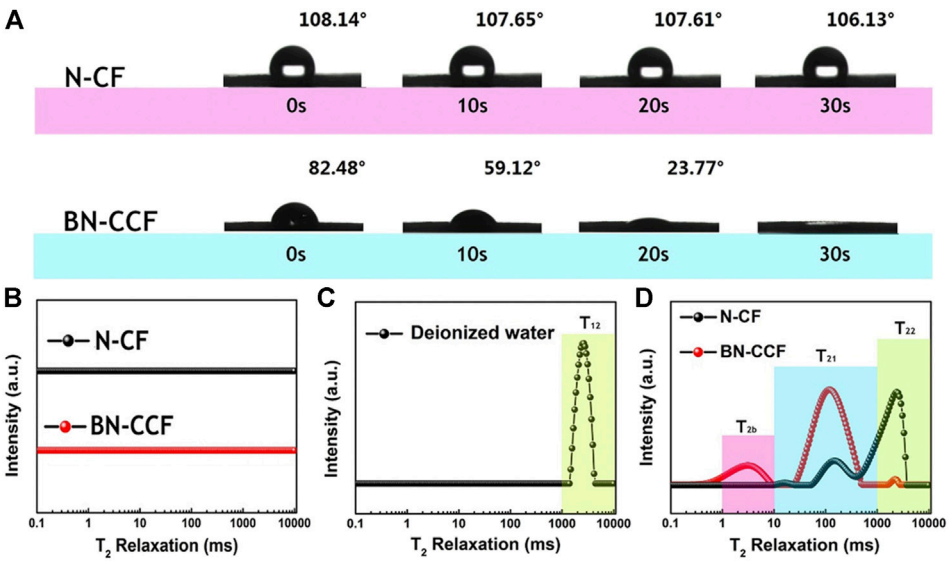

FIGURE 5 | (A) Photographs of dynamic contact angles for the water droplet on N-CF and BN-CCF. T_2 relaxation time distributions for **(B)** N-CF and BN-CCF **(C)** deionized water and **(D)** N-CF and BN-CCF mixed with deionized water.

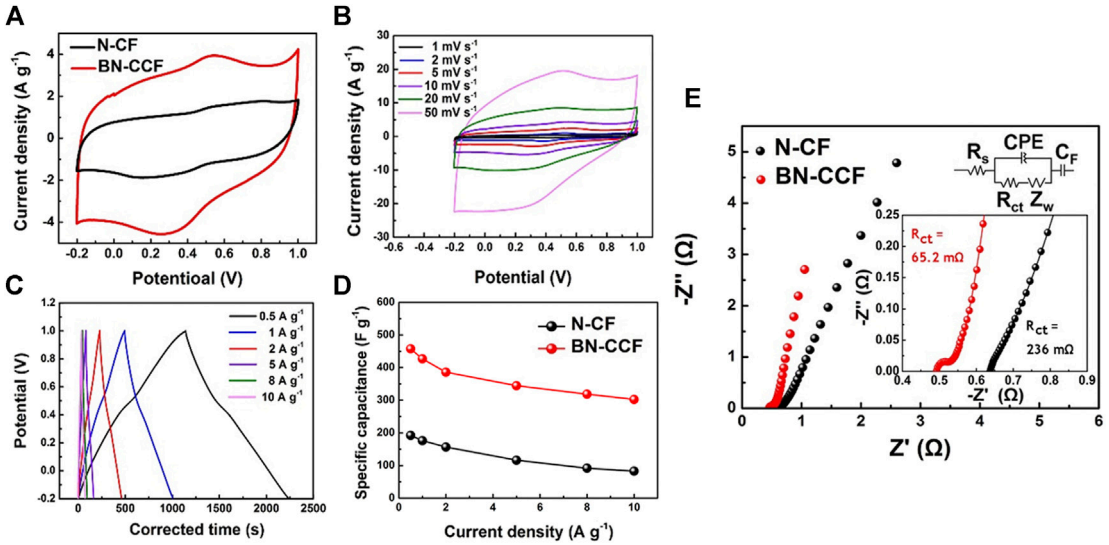

FIGURE 6 | Electrochemical performances of N-CF and BN-CCF: **(A)** CV (10 mV s^{-1}) and **(B)** GCD (1–10 A g^{-1}) curves of N-CF and BN-CCF **(C)** CV (1–50 mV s^{-1}) and **(D)** GCD (0.5–10 A g^{-1}) curves of BN-CCF **(E)** Corresponding equivalent circuit model and Nyquist plots of N-CF and BN-CCF.

TABLE 3 | Comparison of specific capacitance of BN-CCF with other B, N dual doped carbons reported in the literatures.

Sample	C (F g^{-1})	Electrolyte	Current density (A g^{-1})	Ref
BCN nanosheets	244	1 M H_2SO_4	1 A g^{-1}	Chem. Eur. J. 22 (2016) 7134–7140
B, N dual doped carbon nanosheets	240	1 M H_2SO_4	0.1 A g^{-1}	Adv. Funct. Mater. 26 (2016) 111–119
B, N dual doped carbon networks	214	6 M KOH	0.2 A g^{-1}	Carbon 103 (2016) 9–15
B, N dual doped porous carbon	304	1 M H_2SO_4	0.1 A g^{-1}	Carbon 113 (2017) 266–273
B, N dual doped porous carbon foam	402	6 M KOH	0.5 A g^{-1}	ACS Sustain. Chem. Eng. 6 (2018) 11441–11449
B, N dual doped chitosan-derived porous carbons	306	1 M H_2SO_4	0.1 A g^{-1}	Nanoscale 7 (2015) 5120–5125
B, N dual doped carbon nanosphere	423	1 M H_2SO_4	0.2 A g^{-1}	J. Mater. Chem. A 6 (2018) 8053–8058
B, N dual doped porous carbon nanowires	504	1 M H_2SO_4	1 A g^{-1}	J. Power Sources 400 (2018) 264–276
B, N dual doped hollow carbon microspheres	221.5	2 M KOH	1 A g^{-1}	J. Colloid Inter. Sci. 573 (2020) 232–240
B, N dual doped porous carbon	120	6 M KOH	0.5 A g^{-1}	J. Energy Storage 32 (2020) 101706
B, N dual doped coral-like carbon frameworks	457.5	1 M H_2SO_4	0.5 A g^{-1}	This work

relaxation time distributions of N-CF and BN-CCF without adding water. There are no peaks to be found, meaning no water species on the surface of the samples. **Figure 5C** shows the T_2 relaxation time distributions for free water with a single peak centered at 1,000–10,000 ms (T_{22}). As observed from the T_2 relaxation time distributions for N-CF and BN-CCF mixed with deionized water in **Figure 5D**, T_{2b} component (1–10 ms) for BN-CCF shows that the water is closely associated with the surface of BN-CCF, presented as the short T_2 relaxation time distribution centered at 1–10 ms. Correspondingly, N-CF possesses a small part of T_2 relaxation time distribution centered at approximately 10–20 ms, much longer than that for BN-CCF, indicating that the water is bound more loosely on the surface of N-CF. In particular, the T_{21} component (10–1,000 ms) relaxation times follow the order: N-CF > BN-CCF, which means the better ability of water trapped within BN-CCF framework than N-CF. Thus, most of the added water trapped within the BN-CCF framework, displayed a larger peak in T_2 relaxation time distribution centered at 10–1,000 ms (T_{21}). However, for most of the added water in N-CF, the T_2 relaxation time distribution is situated at 1,000–10,000 ms (T_{22}), meaning that the water exists in the state of free water outside of the N-CF framework. Therefore, in other words, the added water can more quickly infiltrate into and trapped within the BN-CCF framework, which is consistent to dynamic water contact angle measurements. The above results confirm that the B-containing groups (B-O, BC_2O, BCO_2, and B-N-C) can improve the affinity of carbon toward aqueous electrolyte, which should play an important role in improving supercapacitive performance of BN-CCF.

The electrochemical performances of N-CF and BN-CCF were investigated in a three-electrode configuration. In **Figure 6A**, CV curves of N-CF and BN-CCF exhibit distorted rectangular shape, but the one of BN-CCF exhibits obviously a pair of redox peaks located at 0.3 V (charge process) and 0.5 V (discharge process), owing to the B-containing groups (B-O, BC_2O, BCO_2, and B-N-C) induced rapid protonation and deprotonation at the interface between electrolyte and BN-CCF based electrode, indicating a pseudocapacitve contribution (Hao et al., 2018; Zhao and Xie,

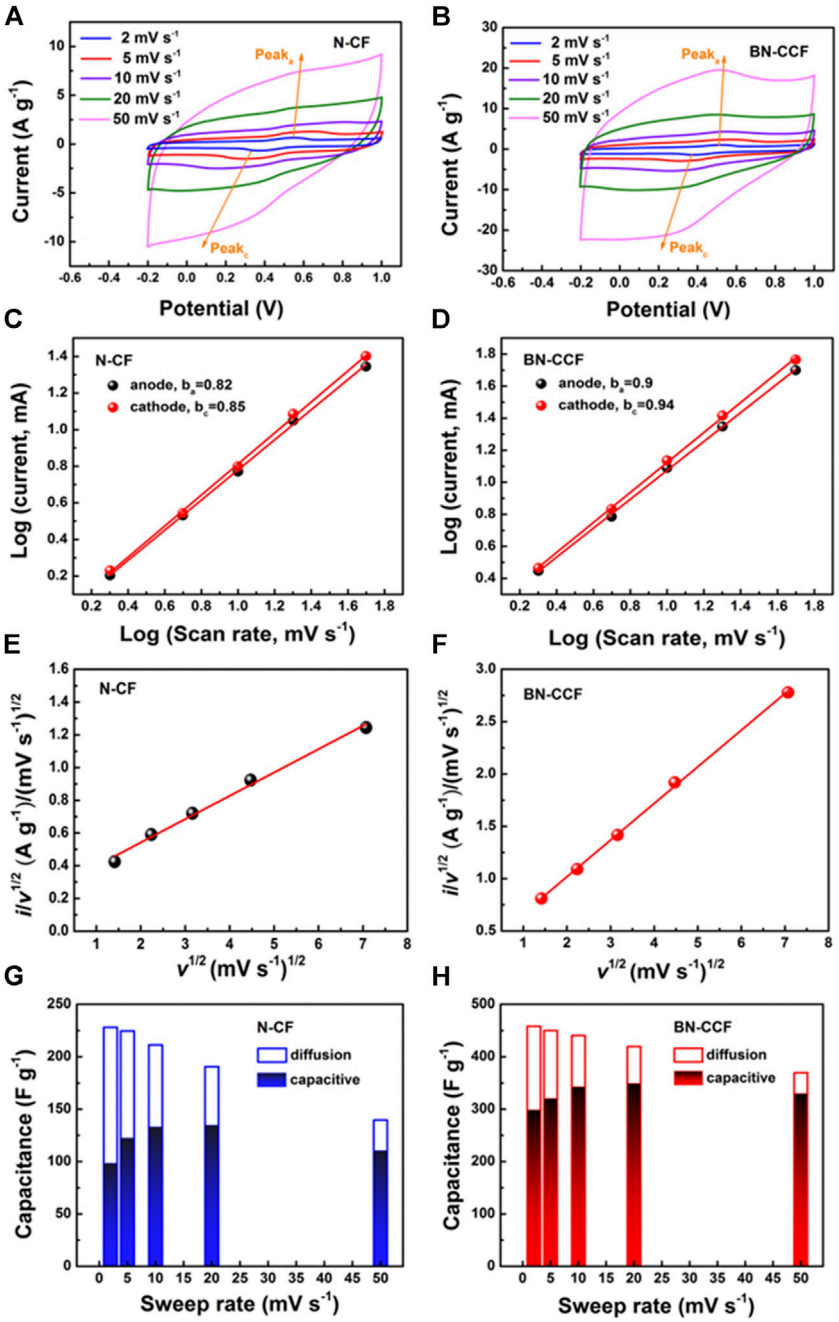

FIGURE 7 | (A,B) CV curves of N-CF and BN-CCF at 2–50 mV s^{-1} **(C,D)** Log(*i*) vs. log(*v*) and **(E,F)** $v^{1/2}$ vs. $i/v^{1/2}$ plots of N-CF and BN-CCF **(G,H)** Capacitive and diffusion-controlled contribution ratios of N-CF and BN-CCF.

TABLE 4 | Capacitive/diffusion-controlled contributions of N-CF and BN-CCF at different scan rates.

Scan rates (mV s^{-1})	2	5 (%)	10 (%)	20 (%)	50 (%)
N-CF/Capacitive contributions	43.2%	54.6	61	70.7	79.1
N-CF/Diffusion-controlled contributions	56.8%	45.4	39	29.3	20.9
BN-CCF/Capacitive contributions	61%	71	77.6	83.1	89.2
BN-CCF/Diffusion-controlled contributions	39%	29	22.4	16.9	10.8

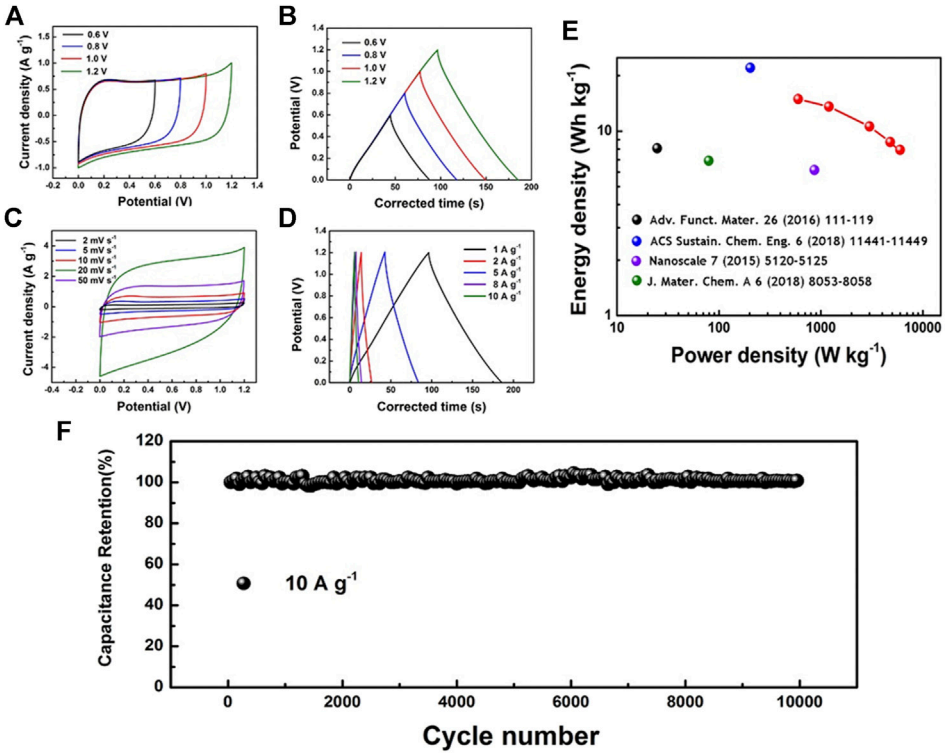

FIGURE 8 | Electrochemical performances of BN-CCF based symmetrical SCs: **(A)** CV curves (10 mV s^{-1}) and **(B)** GCD curves (1 A g^{-1}) in 0.6–1.2 V **(C)** CV curves at different scan rates and **(D)** GCD curves at various current densities in a voltage window of 0–1.2 V **(E)** Ragone plots and **(F)** Cycling performance of BN-CCF based symmetrical SCs.

2018). Meanwhile, BN-CCF exhibits larger integral area than N-CF in CV curves, this is mainly due to the enhanced surface wettability caused by B-containing groups (B-O, BC_2O, BCO_2, and B-N-C) and high accessible surface area of coral-like porous structure. In **Figure 6B**, CV curves of BN-CCF at scan rates (1–50 mV s^{-1}) also show a pair of redox peaks at around 0.3 V (charge process) and 0.5 V (discharge process) (Hao et al., 2018). This distinctive shape remains unchanged at various scan rates, confirming the fast charge/discharge process for faradic reactions and electrical double layer formation over the BN-CCF framework. From GCD profiles in **Figure 6C**, the average specific capacitances of BN-CCF are 457.5, 426.7, 385.9, 344.4, 318.4, and 302.5 F g^{-1} at current densities of 0.5, 1, 2, 5, 8, and 10 A g^{-1}, respectively. And when the current density increases from 0.5 to 10 A g^{-1}, its capacitance retention can reach high 66.1%. As shown in **Figure 6D**, BN-CCF exhibits higher specific capacitances than N-CF at all current densities. EIS measurement results and equivalent circuit model are shown in **Figure 6E**. The fitted charge-transfer resistance (R_{ct}) values of N-CF and BN-CCF are 236 and 65.2 mΩ, respectively. The lower R_{ct} means BN-CCF can facilitate the charge transfer between the electrode and the electrolyte. This is mainly due to the synergistic effect of B, N dual doping, which can reform electron distribution and enhance the hydrophilicity of BN-CCF by introducing B-containing groups (B-O, BC_2O, BCO_2, and B-N-C). Therefore, BN-CCF can exhibit outstanding electrochemical supercapacitive performance. **Table 3** show comparison of specific capacitances of BN-CCF with various reported B, N dual doped carbon materials in the literatures. The BN-CCF framework in this work exhibits higher specific capacitance (457.5 F g^{-1} at 0.5 A g^{-1}) than most of the reported B, N dual doped carbon materials mainly due to its unique coral-like network structure to offer rich ion-accessible surface area and favor the ion diffusion.

In order to explore the capacitive contributions of N-CF and BN-CCF, the corresponding electrochemical kinetics was further investigated, according to the CV curves (2–50 mV s^{-1}) of N-CF and BN-CCF in **Figures 7A,B**. And in **Figures 7C,D**, based on cathodic and anodic peak currents, the electrochemical kinetics could be analyzed by plotting log(*i*) vs. log(*v*) (Kong et al., 2015; Song et al., 2018). The calculated b values of N-CF are 0.82 and 0.85 for the anodic ($peak_a$) and cathodic ($peak_c$) processes, while the corresponding b values of BN-CCF are 0.9 and 0.94, respectively. According to b values analysis above, BN-CCF possesses more significant capacitive behavior than N-CF (Kong et al., 2015), confirming the fast surface kinetics for faradic reactions of B-containing groups (B-O, BC_2O, BCO_2, and B-N-C) over the BN-CCF framework. **Figures 7G,H** show the calculated results of capacitive contributions at various scan rates, on the basis of slopes in **Figures 7E,F**. As shown in **Table 4**, the capacitive contributions of BN-CCF are calculated to be 61, 71, 77.6, 83.1, and 89.2%, at scan rates of 2, 5, 10, 20, and 50 mV s^{-1}, while the

corresponding capacitive contributions of N-CF are calculated to be 43.2, 54.6, 61, 70.7, and 79.1%, respectively. Therefore, when the scan rate changes from 2 to 50 mV s^{-1}, the capacitive contribution of BN-CCF increases from 61 to 89.2%, while the capacitive contribution of N-CF increases from 43.2 to 79.1%. The more significant capacitive contribution of BN-CCF than N-CF is mainly due to pseudocapacitance contribution by fast surface faradic reactions of B-containing groups (B-O, BC_2O, BCO_2, and B-N-C) over the BN-CCF framework.

Symmetrical SC_S were assembled by BN-CCF electrodes (BN-SSC) using 1 M H_2SO_4 electrolyte to further evaluate the practical applications of BN-CCF. In **Figure 8A**, CV curves of BN-SSC exhibit good stability in different potential windows (0.6–1.2 V). And in **Figure 8B**, the corresponding GCD curves of BN-SSC in 0.6–1.2 V at 1 A g^{-1} shows excellent capacitive performance. **Figure 8C** displays the CV curves of BN-SSC in 1.2 V at 2–50 mV s^{-1}, which exhibit similar shapes at all scan rates. The electrochemical performance of BN-SSC was investigated by GCD measurements at various current densities (1–10 A g^{-1}) in **Figure 8D**. The typical CV and GCD curves also indicate good capacitive behavior and rate capability of BN-SSC, which can reach 79.3 F g^{-1} at 1 A g^{-1} and 39.6 F g^{-1} at 10 A g^{-1}. Ragone plots of BN-SSC can be obtained in **Figure 8E**, which possess a high energy density of 14.92 Wh kg^{-1} at a low power density of 600 W kg^{-1}.

The BN-SSC exhibits higher energy density than most of the carbon-based SCs (5–10 Wh kg^{-1}), indicating BN-CCF possesses more excellent electrochemical energy storage performance than similar B, N dual doped carbon (B, N dual doped carbon nanosheets, B, N dual doped porous carbon foam, B, N dual doped chitosan-derived porous carbons, and B, N dual doped carbon nanosphere). **Figure 8F** displays the cycling stability of BN-SSC at 10 A g^{-1} for 10,000 cycles with a capacitance retention of nearly 100%, and **Supplementary Figure S1** shows EIS measurement of BN-CCF before and after long-cycle with similar R_{ct}, exhibiting its excellent cycling stability.

CONCLUSION

In conclusion, superiorly hydrophilic BN-CCF was fabricated *via* a simple calcinating method, which exhibits excellent supercapacitive performance with 457.5 F g^{-1} at 0.5 A g^{-1} and outstanding cycling stability after 10,000 charge-discharge cycles. BN-CCF based symmetrical supercapacitor shows a high energy density of 14.92 Wh kg^{-1} at the power density of 600 W kg^{-1}. The excellent supercapacitive performances are mainly attributed to the coral-like porous structure and superior hydrophilicity that is investigated *via* LF-NMR. And enhanced pseudocapacitance of BN-CCF is caused by the presence of B-containing groups (B-O, BC_2O, BCO_2, and B-N-C) from B, N dual doping. The proposed rational carbons surface structure design and regulation should be considered as an effective strategy to enhance energy storage capacity of carbon-based supercapacitors.

DATA AVAILABILITY STATEMENT

The original contributions presented in the study are included in the article/**Supplementary Material**, further inquiries can be directed to the corresponding author.

AUTHOR CONTRIBUTIONS

LH, XC, and MX contributed to conception and design of the study. LL, HW, and ZH contributed to investigation. LH and ZY organized and analyzed the experimental data and characterizations. SZ, JL, and ZW contributed to validation and data curation. LH wrote the first draft of the manuscript. All authors contributed to manuscript revision, read and approved the submitted version.

FUNDING

Financial support from National Natural Science Foundation of China (No. 21875068) and the Beijing Smart-Chip Microelectronics Technology Co., Ltd. is gratefully acknowledged.

SUPPLEMENTARY MATERIAL

The Supplementary Material for this article can be found online at: https://www.frontiersin.org/articles/10.3389/fmats.2021.705930/full#supplementary-material

REFERENCES

Chang, Z.-H., Feng, D.-Y., Huang, Z.-H., and Liu, X.-X. (2018). Electrochemical Deposition of Highly Loaded Polypyrrole on Individual Carbon Nanotubes in Carbon Nanotube Film for Supercapacitor. *Chem. Eng. J.* 337, 552–559. doi:10.1016/j.cej.2017.12.095

Chen, H., Xiong, Y., Yu, T., Zhu, P., Yan, X., Wang, Z., et al. (2017). Boron and Nitrogen Co-doped Porous Carbon with a High Concentration of boron and its superior Capacitive Behavior. *Carbon* 113, 266–273. doi:10.1016/j.carbon.2016.11.035

Chen, Z., Zhao, S., Zhao, H., Zou, Y., Yu, C., and Zhong, W. (2021). Nitrogen-doped Interpenetrating Porous Carbon/graphene Networks for Supercapacitor Applications. *Chem. Eng. J.* 409, 127891. doi:10.1016/j.cej.2020.127891

Cheng, F., Yang, X., Zhang, S., and Lu, W. (2020). Boosting the Supercapacitor Performances of Activated Carbon with Carbon Nanomaterials. *J. Power Sourc.* 450, 227678. doi:10.1016/j.jpowsour.2019.227678

Du, J., Liu, L., Yu, Y., Lv, H., Zhang, Y., and Chen, A. (2019). Confined Pyrolysis for Direct Conversion of Solid Resin Spheres into Yolk-Shell Carbon Spheres for Supercapacitor. *J. Mater. Chem. A.* 7, 1038–1044. doi:10.1039/c8ta10266j

Geng, Q., Huang, G., Liu, Y., Li, Y., Liu, L., Yang, X., et al. (2019). Facile Synthesis of B/N Co-doped 2D Porous Carbon Nanosheets Derived from Ammonium Humate for Supercapacitor Electrodes. *Electrochimica Acta* 298, 1–13. doi:10.1016/j.electacta.2018.12.038

Gu, B., Su, H., Chu, X., Wang, Q., Huang, H., He, J., et al. (2019). Rationally Assembled Porous Carbon Superstructures for Advanced Supercapacitors. *Chem. Eng. J.* 361, 1296–1303. doi:10.1016/j.cej.2019.01.007

Guo, D., Ding, B., Hu, X., Wang, Y., Han, F., and Wu, X. (2018). Synthesis of Boron and Nitrogen Codoped Porous Carbon Foam for High Performance Supercapacitors. *ACS Sustain. Chem. Eng.* 6, 11441–11449. doi:10.1021/acssuschemeng.8b01435

Hao, G.-P., Mondin, G., Zheng, Z., Biemelt, T., Klosz, S., Schubel, R., et al. (2015). Unusual Ultra-hydrophilic, Porous Carbon Cuboids for Atmospheric-Water Capture. *Angew. Chem. Int. Ed.* 54, 1941–1945. doi:10.1002/anie.201409439

Hao, J., Wang, J., Qin, S., Liu, D., Li, Y., and Lei, W. (2018). B/N Co-doped Carbon Nanosphere Frameworks as High-Performance Electrodes for Supercapacitors. *J. Mater. Chem. A.* 6, 8053–8058. doi:10.1039/c8ta00683k

Hu, M., Zhang, H., Hu, T., Fan, B., Wang, X., and Li, Z. (2020). Emerging 2D MXenes for Supercapacitors: Status, Challenges and Prospects. *Chem. Soc. Rev.* 49, 6666–6693. doi:10.1039/d0cs00175a

Huo, S., Liu, M., Wu, L., Liu, M., Xu, M., Ni, W., et al. (2019). Synthesis of Ultrathin and Hierarchically Porous Carbon Nanosheets Based on Interlayer-Confined Inorganic/organic Coordination for High Performance Supercapacitors. *J. Power Sourc.* 414, 383–392. doi:10.1016/j.jpowsour.2019.01.028

Jian, S.-L., Hsiao, L.-Y., Yeh, M.-H., and Ho, K.-C. (2019). Designing a Carbon Nanotubes-Interconnected ZIF-Derived Cobalt Sulfide Hybrid Nanocage for Supercapacitors. *J. Mater. Chem. A.* 7, 1479–1490. doi:10.1039/c8ta07686c

Kong, L., Zhang, C., Wang, J., Qiao, W., Ling, L., and Long, D. (2015). Free-Standing T-Nb2O5/Graphene Composite Papers with Ultrahigh Gravimetric/Volumetric Capacitance for Li-Ion Intercalation Pseudocapacitor. *ACS Nano* 9, 11200–11208. doi:10.1021/acsnano.5b04737

Lai, S., Zhu, J., Zhang, W., Jiang, J., and Li, X. (2021). Ultralong-Life Supercapacitors Using Pyridine-Derived Porous Carbon Materials. *Energy Fuels* 35, 3407–3416. doi:10.1021/acs.energyfuels.0c03286

Li, D., Chang, G., Zong, L., Xue, P., Wang, Y., Xia, Y., et al. (2019a). From Double-helix Structured Seaweed to S-Doped Carbon Aerogel with Ultra-high Surface Area for Energy Storage. *Energ. Storage Mater.* 17, 22–30. doi:10.1016/j.ensm.2018.08.004

Li, P., Shang, T., Dong, X., Li, H., Tao, Y., and Yang, Q. H. (2021). A Review of Compact Carbon Design for Supercapacitors with High Volumetric Performance. *Small* 17, e2007548, doi:10.1002/smll.202007548

Li, X.-X., Liu, S., Su, W., Cai, L., and Li, J. (2017). Physical Quality Changes of Precooked Chinese Shrimp Fenneropenaeus Chinensis and Correlation to Water Distribution and Mobility by Low-Field NMR during Frozen Storage. *J. Food Process. Pres. Eng.* 41, e13220. doi:10.1111/jfpp.13220

Li, X., Song, Y., You, L., Gao, L., Liu, Y., Chen, W., et al. (2019b). Synthesis of Highly Uniform N-Doped Porous Carbon Spheres Derived from Their Phenolic-Resin-Based Analogues for High Performance Supercapacitors. *Ind. Eng. Chem. Res.* 58, 2933–2944. doi:10.1021/acs.iecr.8b04823

Li, Y., Zhu, G., Huang, H., Xu, M., Lu, T., and Pan, L. (2019c). A N, S Dual Doping Strategy via Electrospinning to Prepare Hierarchically Porous Carbon Polyhedra Embedded Carbon Nanofibers for Flexible Supercapacitors. *J. Mater. Chem. A.* 7, 9040–9050. doi:10.1039/c8ta12246f

Ling, Z., Wang, G., Zhang, M., Fan, X., Yu, C., Yang, J., et al. (2015). Boric Acid-Mediated B,N-codoped Chitosan-Derived Porous Carbons with a High Surface Area and Greatly Improved Supercapacitor Performance. *Nanoscale* 7, 5120–5125. doi:10.1039/c5nr00081e

Ling, Z., Wang, Z., Zhang, M., Yu, C., Wang, G., Dong, Y., et al. (2016). Sustainable Synthesis and Assembly of Biomass-Derived B/N Co-doped Carbon Nanosheets with Ultrahigh Aspect Ratio for High-Performance Supercapacitors. *Adv. Funct. Mater.* 26, 111–119. doi:10.1002/adfm.201504004

Liu, M.-R., Hong, Q.-L., Li, Q.-H., Du, Y., Zhang, H.-X., Chen, S., et al. (2018a). Cobalt boron Imidazolate Framework Derived Cobalt Nanoparticles Encapsulated in B/N Codoped Nanocarbon as Efficient Bifunctional Electrocatalysts for Overall Water Splitting. *Adv. Funct. Mater.* 28, 1801136. doi:10.1002/adfm.201801136

Liu, S., Zhao, Y., Zhang, B., Xia, H., Zhou, J., Xie, W., et al. (2018b). Nano-micro Carbon Spheres Anchored on Porous Carbon Derived from Dual-Biomass as High Rate Performance Supercapacitor Electrodes. *J. Power Sourc.* 381, 116–126. doi:10.1016/j.jpowsour.2018.02.014

Osman, S., Senthil, R. A., Pan, J., and Sun, Y. (2019). A Novel Coral Structured Porous-like Amorphous Carbon Derived from Zinc-Based Fluorinated Metal-Organic Framework as superior Cathode Material for High Performance Supercapacitors. *J. Power Sourc.* 414, 401–411. doi:10.1016/j.jpowsour.2019.01.026

Reece, R., Lekakou, C., and Smith, P. A. (2020). A High-Performance Structural Supercapacitor. *ACS Appl. Mater. Inter.* 12, 25683–25692. doi:10.1021/acsami.9b23427

Saha, S., Jana, M., Khanra, P., Samanta, P., Koo, H., Murmu, N. C., et al. (2015). Band gap Engineering of boron Nitride by Graphene and its Application as Positive Electrode Material in Asymmetric Supercapacitor Device. *ACS Appl. Mater. Inter.* 7, 14211–14222. doi:10.1021/acsami.5b03562

Song, Z., Li, W., Bao, Y., Sun, Z., Gao, L., Nawaz, M. H., et al. (2018). A New Route to Tailor High Mass Loading All-Solid-State Supercapacitor with Ultra-high Volumetric Energy Density. *Carbon* 136, 46–53. doi:10.1016/j.carbon.2018.04.036

Su, H., Huang, H., Zhang, H., Chu, X., Zhang, B., Gu, B., et al. (2018). *In Situ* direct Method to Massively Prepare Hydrophilic Porous Carbide-Derived Carbons for High-Performance Supercapacitors. *ACS Appl. Energ. Mater.* 1, 3544–3553. doi:10.1021/acsaem.8b00764

Sun, F., Qu, Z., Gao, J., Wu, H. B., Liu, F., Han, R., et al. (2018). *In Situ* doping boron Atoms into Porous Carbon Nanoparticles with Increased Oxygen Graft Enhances Both Affinity and Durability toward Electrolyte for Greatly Improved Supercapacitive Performance. *Adv. Funct. Mater.* 28, 1804190. doi:10.1002/adfm.201804190

Wang, J.-G., Liu, H., Zhang, X., Shao, M., and Wei, B. (2018). Elaborate Construction of N/S-co-doped Carbon Nanobowls for Ultrahigh-Power Supercapacitors. *J. Mater. Chem. A.* 6, 17653–17661. doi:10.1039/c8ta07573e

Wang, S., Ma, F., Jiang, H., Shao, Y., Wu, Y., and Hao, X. (2018). Band gap-tunable Porous Borocarbonitride Nanosheets for High Energy-Density Supercapacitors. *ACS Appl. Mater. Inter.* 10, 19588–19597. doi:10.1021/acsami.8b02317

Wang, Y., Tao, S., An, Y., Wu, S., and Meng, C. (2013). Bio-inspired High Performance Electrochemical Supercapacitors Based on Conducting Polymer Modified Coral-like Monolithic Carbon. *J. Mater. Chem. A.* 1, 8876–8887. doi:10.1039/c3ta11348e

Wiesman, Z., Linder, C., Resende, M. T., Ayalon, N., Levi, O., Bernardinelli, O. D., et al. (2018). 2D and 3D Spectrum Graphics of the Chemical-Morphological Domains of Complex Biomass by Low Field Proton NMR Energy Relaxation Signal Analysis. *Energy Fuels* 32, 5090–5102. doi:10.1021/acs.energyfuels.7b03339

Xia, Q., Yang, H., Wang, M., Yang, M., Guo, Q., Wan, L., et al. (2017). High Energy and High Power Lithium-Ion Capacitors Based on boron and Nitrogen Dual-Doped 3D Carbon Nanofibers as Both Cathode and Anode. *Adv. Energ. Mater.* 7, 1701336. doi:10.1002/aenm.201701336

Xiao, Q., Zhao, Z., and Lim, L.-T. (2018). Structure Evolution of Pullulan-Alginate Edible Films during Drying Studied by Low-Field NMR. *J. Food Process. Pres. Eng.* 41, e12636. doi:10.1111/jfpe.12636

Yi, R., Chen, S., Song, J., Gordin, M. L., Manivannan, A., and Wang, D. (2014). High-Performance Hybrid Supercapacitor Enabled by a High-Rate Si-Based Anode. *Adv. Funct. Mater.* 24, 7433–7439. doi:10.1002/adfm.201402398

Yoo, H., Min, M., Bak, S., Yoon, Y., and Lee, H. (2014). A Low Ion-Transfer Resistance and High Volumetric Supercapacitor Using Hydrophilic Surface Modified Carbon Electrodes. *J. Mater. Chem. A.* 2, 6663–6668. doi:10.1039/c4ta00158c

Yue, J., Zhang, H., Zhang, Y., Li, M., and Zhao, H. (2020). Coral-like Carbon Structures Derived from the Complex of Metal-Organic Frameworks and Melamine Formaldehyde Resin with Ideal Electrochemical Performances. *Electrochimica Acta* 353, 136528. doi:10.1016/j.electacta.2020.136528

Zhang, H., Zhang, Z., Luo, J. D., Qi, X. T., Yu, J., Cai, J. X., et al. (2019). A Chemical Blowing Strategy to Fabricate Biomass-Derived Carbon-Aerogels with Graphene-like Nanosheet Structures for High-Performance Supercapacitors. *ChemSusChem* 12, 2462–2470. doi:10.1002/cssc.201802245

Zhang, J., Nie, N., Liu, Y., Wang, J., Yu, F., Gu, J., et al. (2015). Boron and Nitrogen Codoped Carbon Layers of LiFePO4Improve the High-Rate Electrochemical

Performance for Lithium Ion Batteries. *ACS Appl. Mater. Inter.* 7, 20134–20143. doi:10.1021/acsami.5b05398

Zhang, J., Sun, Y., Zhu, J., Kou, Z., Hu, P., Liu, L., et al. (2018). Defect and Pyridinic Nitrogen Engineering of Carbon-Based Metal-free Nanomaterial toward Oxygen Reduction. *Nano Energy* 52, 307–314. doi:10.1016/j.nanoen.2018.08.003

Zhao, J., Lai, H., Lyu, Z., Jiang, Y., Xie, K., Wang, X., et al. (2015). Hydrophilic Hierarchical Nitrogen-Doped Carbon Nanocages for Ultrahigh Supercapacitive Performance. *Adv. Mater.* 27, 3541–3545. doi:10.1002/adma.201500945

Zhao, Z., and Xie, Y. (2018). Electrochemical Supercapacitor Performance of boron and Nitrogen Co-doped Porous Carbon Nanowires. *J. Power Sourc.* 400, 264–276. doi:10.1016/j.jpowsour.2018.08.032

Zhu, Q., Zhao, D., Cheng, M., Zhou, J., Owusu, K. A., Mai, L., et al. (2019). A New View of Supercapacitors: Integrated Supercapacitors. *Adv. Energ. Mater.* 9, 1901081. doi:10.1002/aenm.201901081

Conflict of Interest: Authors XC, SZ, JL, ZW, LL, HW, and ZH are employed by the company Beijing Smart-Chip Microelectronics Technology Co., Ltd.

The remaining authors declare that the research was conducted in the absence of any commercial or financial relationships that could be construed as a potential conflict of interest.